HIGH RESOLUTION NUMERICAL MODELS OF CORONA FORMATION INTEGRATING MAGMATIC PROCESSES, SURFACE FRACTURING, AND ECLOGITIZATION. J. Schools[1,2] and S. E. Smrekar[2], [1]NASA Postdoctoral Program Fellow, [2]Jet Propulsion Laboratory, California Institute of Technology, Pasadena, CA (joseph.w.schools@jpl.nasa.gov; suzanne.e.smrekar@jpl.nasa.gov).

Introduction: Coronae are quasicircular volcanic-tectonic features plentiful and seemingly unique to the surface of Venus [1,2]. They are generally defined by an annulus of surface fractures [3] and are typically 100 to 1000 km in diameter (2600 km at the largest). Coronae are geologically complex, and can include any combination of volcanic domes, one or more annulus of discontinuous ridges, and extensive (10^4-10^6 km^2) lava flows [4]. Some large corona display deep, narrow trenches hypothesized to be evidence of subduction [5].

Most proposed formation mechanisms of corona involve some kind of uplift followed by a collapse that creates the fracture patterns and ridge topography [e.g. 6]. As evidenced by the volcanic domes and lava flows, magmatic processes are clearly present in the formation of corona, however the role of mantle derived melt and the resulting magmatic/volcanic processes is currently understudied due to the computational complexity of melt dynamics. Here we present a model of corona formation integrating a brittle visco-plastic rheology with two-phase flow melt migration and eclogite phase changes.

Model: We use a modified version of the finite element code ASPECT 2.4 [7,8], integrating a visco-plastic rheology [9] with the existing two-phase flow melt migration physics [10]. For models with melt migration ASPECT operates by solving a series of equations representing the behavior of silicate melt moving through and interacting with a viscously deforming host rock. The initial solid ductile shear viscosity is calculated as an inverse average of the diffusion creep and dislocation creep, based on set rheological flow laws:

$$\frac{1}{\eta_0} = \frac{1}{\eta_{\text{diffusion}}} + \frac{1}{\eta_{\text{dislocation}}} \quad (1)$$

The ductile shear viscosity is then modified based on the presence of melt:

$$\eta = \eta_0 \exp(-\alpha_\phi \phi) \quad (2)$$

where ϕ is the porosity and α_ϕ is a constant. Brittle failure is modeled as a reduction in viscosity when a yield stress is reached:

$$\eta_{\text{eff}} = \begin{cases} \dfrac{\bar{\tau}_y}{2\dot{\varepsilon}'_{s,II}} & for\ \bar{\tau}_{II} = \bar{\tau}_y \\ \eta & for\ \bar{\tau}_{II} < \bar{\tau}_y \end{cases} \quad (3)$$

where $\dot{\varepsilon}'_{s,II}$ is the second invariant of the deviatoric strain rate, $\bar{\tau}_y$ is a calculated yield stress, and $\bar{\tau}_{II}$ is the second invariant of the shear stress. Due to the presence of melt in the models, similar calculations are performed for the compaction viscosity:

$$\xi = \frac{\eta_0}{\phi} \quad (4)$$

$$\xi_{\text{eff}} = \begin{cases} -\dfrac{P_y}{\dot{v}_s} & for\ P_c \le P_y \\ \xi & for\ P_c > P_y \end{cases} \quad (5)$$

Where P_y is a calculated yield pressure, $\dot{v}_s$ is the volumetric strain rate, and P_c is the compaction pressure. This formulation for visco-plastic deformation allows for processes such as melt induced cracking, but more importantly allows for the model to simultaneously solve surface fracturing at the surface as well as melt processes at depth. Elastic effects are ignored in this model.

Composition and melting/crystallization are approximated as a function of enrichment and depletion of peridotite [11]. A basalt-eclogite phase change is implemented as a function of temperature, pressure, and composition [12].

Corona formation is modeled in 2D as a hot mantle body (plume) which melts and interacts with the lithosphere and crust as it ascends. Resulting surface topography is recorded through a free surface with mesh deformation at the top boundary of the model [13]. The left boundary pulls material out at a constant velocity, creating a constant background strain rate of 10^{-15} 1/s. The bottom boundary has material flow in to accommodate the mass balance. The right boundary is free slip.

Results: Models were performed with varying values of plume radius (r_{plume}), plume temperature (T_{plume}), lithosphere thickness ($H_{lithosphere}$), and crust thickness (H_{crust}). Most models show an initial topographic rise which spreads laterally as the plume spreads against the base of the lithosphere. As the plume rises, the generated melt rises and accumulates in buoyant regions that create topographic ridges. These ridges move laterally as the plume spreads at the base of the lithosphere. Active surface fractures generally form around the areas of topographic elevation.

Hotter plumes (1888 K) generally support larger topography (>4 km) over shorter timescales (10^4 years). Smaller plumes (50 km radius) generally support smaller topography (0.5-2 km) over larger timescales

(10^5 years).

A subset of lower resolution models observed over larger timescales (10^6 years) show further evolution at the base of the lithosphere, but are not resolved enough to show surface fracturing. In these models, crystallized melt cools and accumulates at the base of the lithosphere. These regions of basaltic composition undergo the eclogite phase change, densify, and begin to drip down from the base of the lithosphere. The surface topography is pulled down forming troughs above the downwellings. In longer running models the preexisting crust is pulled down, and can undergo the eclogite phase change, possibly indicating subduction initiation.

In models given an Earthlike surface temperature (237 K), the same asthenosphere/base of lithosphere processes are observed, however the colder lithosphere is too rigid and forms topography at 100 m scales as opposed to 1 km scales.

Discussion: Modeled corona topography generally matches observed corona morphologies and amplitudes (2-4 km). Surface fracturing is generally located in the same places as observed corona [14], with the exception of the tops of central domes which is favored in the model but seldom observed. Further evolution of corona such as lava flows may mask fracturing in reality.

The model produces several observed corona morphologies (including multiple ridges) over a single run (10^5 years). This may indicate that extant corona represent active magmatic processes occurring over 10^4-10^5 year timescales. Model outputs such as topography, fracture location, and surface heat flow can be compared to future spacecraft data to constrain current Venus interior thermal and compositional structure.

Clear corona examples are not observed on Earth due to the low surface temperature. Subduction initiation may occur on corona edges due to eclogitization of crustal material.

Acknowledgments: This research was supported by an appointment to the NASA Postdoctoral Program at JPL, administered by Oak Ridge Associated Universities under contract with NASA. The authors acknowledge the Texas Advanced Computing Center (TACC) at The University of Texas at Austin for providing HPC and visualization resources. ASPECT is hosted by the Computational Infrastructure for Geodynamics (CIG) which is supported by the National Science Foundation award EAR-1550901.

References: [1] Barsukov V. L. et al. (1986) *JGR Solid Earth, 91*, 378–398. [2] Glaze L. S. et al. (2002) *JGR Planets, 107*, 18-1-18-12. [3] Stofan E. R. et al. (2001) *GRL, 28*, 4267-4270. [4] Roberts K. M. & Head J. W. (1993) *GRL, 20*, 1111-1114. [5] Schubert, G. & Sandwell D. T. (1995) *Icarus, 117*, 173-196. [6] Smrekar, S. E., & Stofan, E. R. (1997) *Science, 277*, 1289-1294. [7] Kronbichler, M. et al. (2012) *GJI, 191*, 12-29. [8] Heister, T. et al. (2017) *GJI, 210*, 833-851. [9] Keller, T. et al. (2013) *GJI, 195*, 1406-1442. [10] Dannberg, J. & Hesiter, T. (2016) *GJI, 207*, 1343-1366. [11] Katz R. F. et al. (2003) *G^3, 4*, 1073 [12] Ito, K. & Kennedy, G. C. (1971) In The Structure and Physical Properties of the Earth's Crust. [13] Rose, I. et al. (2017) *Phys. Earth Planet. Inter., 262*, 90-100. [14] Sabbeth et al. (2023) LPSC 54, Abstract #1769

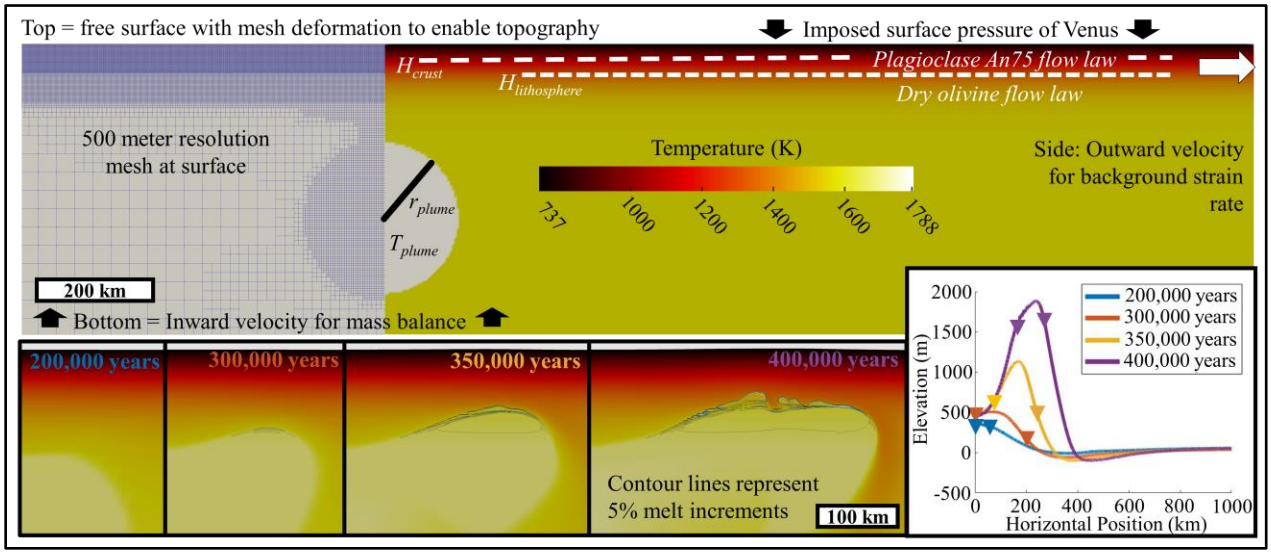

Figure 1 – Top: Model set up. Bottom panels: Selection of timesteps from a model with a 1788 K, 130 km radius plume, a 30 km crust, and a 45 km lithosphere. Bottom plot: Surface topography corresponding to panel timesteps with regions of active surface fracturing denoted between triangles.